

## Supplemental Material

### Sample description and preparation procedures

**Scandium solution.** A ca. 1 wt% Sc solution was prepared by dissolving 0.6 g commercial Sigma–Aldrich  $\text{Sc}^{3+}$  chloride hexahydrate ( $\text{ScCl}_3 \cdot 6\text{H}_2\text{O}$ ) powder – 99.999% into 10 mL of distilled water.

**Scandium-substituted goethite.** Ferrihydrite was precipitated by adding 50 mL  $1.35 \text{ mol} \cdot \text{L}^{-1}$  NaOH to 25 mL  $0.5 \text{ mol} \cdot \text{L}^{-1}$   $\text{Fe}(\text{NO}_3)_3$  and 25 mL of  $1 \text{ mmol} \cdot \text{L}^{-1}$   $\text{ScCl}_3$  solutions. The suspension was then diluted to 1 L with a  $33 \text{ mmol} \cdot \text{L}^{-1}$  NaOH solution. The solution was heated to  $65^\circ\text{C}$  in a water-bath for 48 h, transforming the ferrihydrite suspension into a precipitate of goethite. The solid product was separated by centrifugation, washed at  $45^\circ\text{C}$  for 2 h in a  $3 \text{ mol} \cdot \text{L}^{-1}$   $\text{H}_2\text{SO}_4$  solution, in order to remove any adsorbed species and dried at  $45^\circ\text{C}$  for 24 h giving 1 g of Sc-bearing goethite.

**Scandium-substituted hematite.** Sc-bearing hematite was obtained by dehydroxylation of the previously synthesized goethite at  $300^\circ\text{C}$ .

**Scandium-adsorbed iron oxides.** 10 mL of  $\text{ScCl}_3$  solution at 1000 ppm Sc was added to 1 g of pure goethite or hematite obtained following the synthesis method previously described without addition of  $\text{ScCl}_3$ . The near neutral pH of the solution prohibits any dissolution and precipitation of Sc-bearing goethite and hematite, considering their stability diagram. The solid and the solution were shaken together for 24 h. The solid was then separated by centrifugation and dried at  $45^\circ\text{C}$  for 24 h.

**Adsorption onto montmorillonite.** Scandium-adsorbed montmorillonite was obtained by adding 10 mL of  $\text{ScCl}_3$  solution at 1 wt% Sc to 1 g of pure natural montmorillonite commercialized by Sigma–Aldrich. The solid and the solution were shaken together for 24 h. The solid was then separated by centrifugation and dried at  $45^\circ\text{C}$  for 24 h.

**Lateritic sample.** The sample comes from the Syerston–Flemington lateritic deposit (sample JSD2-125, Chassé et al., 2019). Scandium concentration is ca. 750 ppm (ICP–MS analyses) and Rietveld refinement of X-ray diffraction data indicate that goethite proportion is ca. 27 % while hematite proportion is ca. 36 %, the remaining being mainly kaolinite, known to be inefficient for Sc trapping (Chassé et al., 2017).

**Scandium concentrations.** The amount of Sc of the synthetic Sc-bearing goethite, Sc-bearing hematite, Sc-adsorbed goethite, Sc-adsorbed hematite and Sc-adsorbed montmorillonite has been determined to be  $898 \text{ ppm} \pm 0.025 \%$ ,  $872 \text{ ppm} \pm 0.025 \%$ ,  $819 \text{ ppm} \pm 0.025 \%$  and  $837 \text{ ppm} \pm 0.025 \%$  and  $13,940 \text{ ppm} \pm 0.025 \%$ , respectively. Scandium concentrations were measured by ICP–MS, following the procedure described in Chassé et al. (2019).

### Computational details

In order to model experimental spectra, theoretical XANES spectra were calculated, based on prior successful modeling of Sc K-edge XANES spectra of reference compounds (Chassé et al., 2018), using the QUANTUM ESPRESSO plane-wave based density functional theory (DFT) suite of codes (Giannozzi et al., 2009). We used the generalized gradient approximation (GGA) to the exchange–correlation functional with the Perdew–Burke–Ernzerhof (PBE) parametrization (Perdew et al., 1996). The ionic cores were described by ultrasoft pseudopotentials that have been generated according to a modified Rappe–Rabe–Kaxiras–Joannopoulos scheme (Rappe et al., 1990). Scalar relativistic effects are included in the pseudopotentials. The Sc ultrasoft pseudopotential was generated considering the  $3s$ ,  $3p$ ,  $4s$ ,  $3d$  and  $4p$  states as valence states, with cut-off radii of  $1.30 \cdot a_0$ ,  $1.45 \cdot a_0$ ,  $1.30 \cdot a_0$ ,  $1.50 \cdot a_0$  and  $1.45 \cdot a_0$ , respectively ( $a_0$  is the Bohr radius and  $l = 2$  was taken as the local part). The pseudopotential of the absorbing Sc atom (Sc\*) was generated from the Sc electronic configuration with a single  $1s$  electron. The valence states of the Fe ultrasoft

pseudopotential were the  $4s$ ,  $3d$  and  $4p$  states with cut-off radii of  $2.00 \cdot a_0$ ,  $1.60 \cdot a_0$ ,  $2.20 \cdot a_0$  ( $l = 2$  was taken as the local part). The valence states of the O ultrasoft pseudopotential were the  $2s$ ,  $2p$ ,  $3s$  and  $3p$  states with cut-off radii of  $1.30 \cdot a_0$ ,  $1.35 \cdot a_0$ ,  $1.30 \cdot a_0$  and  $1.35 \cdot a_0$  ( $l = 2$  was taken as the local part). The valence states of the H ultrasoft pseudopotential were the  $1s$  states with a cut-off radius of  $0.90 \cdot a_0$ . The wavefunctions and charge density were expanded in plane waves and the respective cut-offs were set from convergence tests to 40 Ry and 480 Ry. Increasing these energy cut-offs to 50 Ry and 600 Ry did not significantly modify the results. The electronic occupations are smeared with a Gaussian spreading of 0.007 Ry.

For each model detailed below, a relaxation calculation is performed during which atomic positions and magnetic moments are free to relax. The convergence threshold on the total energy for self-consistency is set at  $10^{-9}$  Ry., total energy between two consecutive SCF steps at  $10^{-4}$  Ry and forces at  $10^{-3}$  Ry/ $a_0$ . Following the relaxation, SCF calculations were made with a  $1s$  core hole successively located on each Sc of the supercell. Due to the  $1s$  core hole, the total charge of the supercell is set to +1 (full core hole approach). The Brillouin zone was sampled according to the Monkhorst–Pack scheme (Monkhorst and Pack, 1976), using shifted  $4 \times 4 \times 4$   $k$ -point grid, large enough to provide fully converged results.

In the XSpectra code, the reconstruction of the all-electron wavefunctions is done within the projector augmented wave method (Blöchl, 1994). To be able to treat large cells with about one hundred atoms or more, the scheme uses a recursion method to construct a Lanczos basis and then computes the cross section as a continued fraction. For each compound, the absorption cross sections are calculated in the electric dipole (E1) and quadrupole (E2) approximations, on a  $4 \times 4 \times 4$   $k$ -point grid, with a broadening parameter of 0.43 eV from  $-10$  eV to 5 eV relative to the Fermi level, taking into account the core-hole lifetime (Krause and Oliver, 1979). At higher energies, the photoelectron is fast enough to interact with the electron gas of the system and its

mean free path is consequently attenuated, inducing a sharp decrease in the lifetime behavior (Saintavit et al., 1989). The broadening parameter was increased accordingly up to 3 eV following an arctangent function (Filipponi, 2000) starting at 5 eV with an inflection point at 25 eV above the Fermi level.

In order to interpret the pre-edge XANES features, partial electronic densities of states (DOS) were calculated on the systems having the core hole, using Löwdin projections, a shifted  $4 \times 4 \times 4$  Monkhorst–Pack  $k$ -point grid and a Gaussian broadening of 0.3 eV.

Theoretical spectra are calculated for a given orientation of the polarization vector and, in the E2 approximation, also of the wave vector. However, the experimental spectra are measured on powdered samples and the cross section obtained corresponds to the isotropic cross section. In order to retrieve the isotropic cross section, symmetry considerations have been used (Brouder, 1990). For orthorhombic crystals, such as goethite, by selecting specific orientations of the polarization and wave vectors, only two spectra need to be calculated for the E1 approximation and one for the E2 approximation (Cabaret et al., 2010). For trigonal crystals, such as hematite, one spectrum must be calculated in the E1 approximation and three in the E2 approximation. The demonstration on the number of individual theoretical spectra required to retrieve the isotropic cross sections and the corresponding orientations of the polarization vector and the wave vector is detailed below. To avoid symmetrization issues known to exist in the suite of codes, the calculated spectra have been verified by comparison with spectra containing additional cross sections with supplementary orientations of the polarization and wave vectors.

When two Sc atoms are included in the unit cell, two individual spectra are obtained, one for each Sc of the supercell. They are averaged taking into account the core-level shift (Lelong et al., 2014).

The calculated spectra are then aligned with the experimental ones with respect to the energy position of the main XANES peak.

### **Goethite, hematite and water complex models**

Goethite ( $P 2_1/n 2_1/m 2_1/a$  space group) has an orthorhombic unit cell containing four formula units with the following cell parameters optimized from earlier structure relaxation using similar computational parameters (Blanchard et al., 2014; Ducher et al., 2015):  $a \approx 10.01 \text{ \AA}$ ,  $b \approx 3.03 \text{ \AA}$  and  $c \approx 4.65 \text{ \AA}$ . Goethite is antiferromagnetic; half of the Fe atoms have their spin-up density of states larger than their spin-down density of states and *vice versa*. Spin-up and spin-down cations are found in alternate chains of octahedra that run along the b-axis (Cornell and Schwertmann, 2003).

Hematite ( $R \bar{3} 2/c$  space group) is described in a hexagonal lattice containing six formula units with  $a \approx 5.02 \text{ \AA}$  and  $c \approx 13.90 \text{ \AA}$  (optimized cell parameters taken from Blanchard et al., 2008).

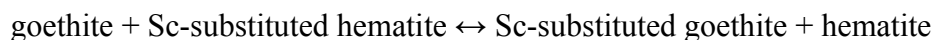
Hematite is antiferromagnetic below the Morin temperature (260 K) with the Fe spins aligning along the  $[111]$  axis of the rhombohedral unit cell. Above the Morin transition and below the Néel temperature, 948 K, hematite shows a weak ferromagnetism due to a slight canting of the spins lying in the basal plane (i.e. the plane perpendicular to the hexagonal c-axis). Beyond 948 K, hematite becomes paramagnetic. All our calculations have been set up with the antiferromagnetic configuration since it is known to be the most stable (Cornell and Schwertmann, 2003).

For Sc adsorbed on Fe oxides, a model of 6-fold coordinated  $[\text{Sc}(\text{H}_2\text{O})_4(\text{OH})_2]^+$  complex was used, following the geometry proposed by (Rudolph and Pye, 2000) from Raman spectroscopic measurements. The reasons for this choice are discussed in the letter.

Considering the size of the mineral cells,  $1 \times 3 \times 2$  orthorhombic and  $2 \times 2 \times 1$  hexagonal supercells were respectively used to model goethite and hematite in order to avoid the interaction of the atom having a core hole with its periodic images. Either one or two adjacent Sc atoms were substituted for Fe atoms in the crystal structures. To avoid interaction with periodic images, the Sc water complex has also been isolated in a large cubic cell ( $a = 20 \text{ \AA}$ ).

Interatomic distances, Fe–O and Sc–O are given for the site of Sc incorporation before and after the substitution of Sc for Fe and the relaxation calculations (Table S1). The energy of structural models of goethite and hematite, either substituted or not, is given after relaxation calculations (Table S2).

From these energies, we can determine the energy ( $\Delta E_{\text{Gt-Hem}}$ ) of the following reaction :



Considering that Sc and Fe sources and sink are the same, that is an aqueous solution infiltrating a lateritic regolith, this energy reaction gives a good approximation of the Gibbs free energy ( $\Delta G$ ) informing on the preferential incorporation of Sc in one Fe oxide or the other.

**Table S1** Interatomic Fe–O and Sc–O distances before and after Sc substitution and percentage of bond length relaxation associated with the Fe-Sc substitution.

**Table S2** Total energy of the structural models of goethite and hematite, either substituted or not, after relaxation.

### Expression of the electric-dipole and electric-quadrupole isotropic cross section

**X-ray polarization vector.** In an orthonormal reference frame bound to the crystal, the X-ray polarization vector is written:

$$\hat{\epsilon} = \begin{pmatrix} \sin \theta \cdot \cos \varphi \\ \sin \theta \cdot \sin \varphi \\ \cos \theta \end{pmatrix} \quad (1)$$

The  $z$  axis is chosen along the  $[001]$  direction of the crystal according to the International Tables for X-Ray Crystallography. The  $x$  axis is taken parallel to the  $[100]$  direction of the crystal.  $\theta$  is the angle of  $\hat{\epsilon}$  relative to the  $z$  axis while  $\varphi$  is the angle of  $\hat{\epsilon}$  relative to the  $x$  axis.

**Trigonal Crystals.** In trigonal crystals with a  $D_{3d}$  point group, the angular dependence of the E1 absorption is dichroic (Brouder, 1990). The E1 cross section,  $\sigma_{D_{3d}}^D(\hat{\epsilon})$ , can be expressed as:

$$\sigma_{D_{3d}}^D(\hat{\epsilon}) = \sigma_{D_{3d}}^D(0, 0) - \frac{1}{\sqrt{2}} \cdot (3 \cdot \cos^2 \theta - 1) \cdot \sigma_{D_{3d}}^D(2, 0) \quad (2)$$

When  $\theta = 0$  and  $\varphi = 0$ , the X-ray polarization vector is:

$$\hat{\epsilon} = \begin{pmatrix} \sin(\arccos \frac{1}{\sqrt{3}}) \\ 0 \\ \frac{1}{\sqrt{3}} \end{pmatrix} = \hat{\epsilon}_1 \quad (3)$$

From equation 2, we show that the E1 isotropic cross section of a trigonal crystal with a  $D_{3d}$  point group is:

$$\sigma_{D_{3d}}^D(0, 0) = \sigma_{D_{3d}}^D(\hat{\epsilon}_1) \quad (4)$$

**Orthorhombic crystals.** In orthorhombic crystals with a  $D_{2h}$  point group, the angular dependence of the E1 absorption is trichroic (Brouder, 1990). The E1 cross section,  $\sigma_{D_{2h}}^D(\hat{\epsilon})$ , can be expressed as:

$$\begin{aligned} \sigma_{D_{2h}}^D(\hat{\epsilon}) = & \sigma_{D_{2h}}^D(0, 0) \\ & - \sqrt{3} \cdot \sin^2 \theta \cdot \cos 2\varphi \cdot \sigma_{D_{2h}}^{Dr}(2, 2) \\ & - \frac{1}{\sqrt{2}} \cdot (3 \cdot \cos^2 \theta - 1) \cdot \sigma_{D_{2h}}^D(2, 0) \end{aligned} \quad (5)$$

When  $\theta = 0$  and  $\varphi = 0$ :

$$\hat{\epsilon} = \begin{pmatrix} 0 \\ 0 \\ 1 \end{pmatrix} = \hat{\epsilon}_1 \quad (6)$$

$$\sigma_{D_{2h}}^D(\hat{\epsilon}_1) = \sigma_{D_{2h}}^D(0, 0) - \frac{2}{\sqrt{2}} \cdot \sigma_{D_{2h}}^D(2, 0) \quad (7)$$

When  $\theta = \frac{\pi}{2}$  and  $\varphi = \frac{\pi}{4}$ :

$$\hat{\epsilon} = \begin{pmatrix} \frac{1}{\sqrt{2}} \\ \frac{1}{\sqrt{2}} \\ 0 \end{pmatrix} = \hat{\epsilon}_2 \quad (8)$$

$$\sigma_{D_{2h}}^D(\hat{\epsilon}_2) = \sigma_{D_{2h}}^D(0, 0) + \frac{1}{\sqrt{2}} \cdot \sigma_{D_{2h}}^{Dr}(2, 0) \quad (9)$$

From equation 7 and 9, we show that the E1 isotropic cross section of an orthorhombic crystal with a  $D_{2h}$  point group is:

$$\sigma_{D_{3h}}^D(0,0) = \frac{\sigma_{D_{3h}}^D(\hat{\epsilon}_1) + 2 \cdot \sigma_{D_{3h}}^D(\hat{\epsilon}_2)}{3} \quad (10)$$

### Expression of the Electric-Quadrupole (E2) Isotropic Cross section

**X-ray polarization vector and wavevector.** The general coordinates of the vectors are:

$$\hat{\epsilon} = \begin{pmatrix} \sin \theta \cdot \cos \varphi \\ \sin \theta \cdot \sin \varphi \\ \cos \theta \end{pmatrix} \quad \hat{k} = \begin{pmatrix} \cos \theta \cdot \cos \varphi \cdot \cos \psi - \sin \varphi \cdot \sin \psi \\ \cos \theta \cdot \sin \varphi \cdot \cos \psi - \cos \varphi \cdot \sin \psi \\ -\sin \theta \cdot \cos \psi \end{pmatrix} \quad (11)$$

The angle  $\psi$  gives the direction of the wavevector in the plane perpendicular to the polarization vector. The orthonormal axes are chosen as in equation 1.

**Trigonal crystals.** For trigonal crystals with a  $D_{3d}$  point group, symmetry considerations lead to the following expression of the E2 absorption cross section (Brouder, 1990):

$$\begin{aligned} \sigma_{D_{3d}}^Q(\hat{\epsilon}, \hat{k}) = & \sigma_{D_{3d}}^Q(0, 0) \\ & + \sqrt{\frac{5}{14}} \cdot (3 \cdot \sin^2 \theta \cdot \sin^2 \psi - 1) \cdot \sigma_{D_{3d}}^Q(2, 0) \\ & + \frac{1}{\sqrt{14}} \cdot (35 \cdot \sin^2 \theta \cdot \cos^2 \theta \cdot \cos^2 \psi + 5 \cdot \sin^2 \theta \cdot \sin^2 \psi - 4) \cdot \sigma_{D_{3d}}^Q(4, 0) \quad (12) \\ & - \sqrt{10} \cdot \sin \theta \cdot [(2 \cdot \cos^2 \theta \cdot \cos^2 \psi - 1) \cdot \cos \theta \cdot \cos 3\varphi \\ & - (3 \cdot \cos^2 \theta - 1) \cdot \sin \psi \cdot \cos \psi \cdot \sin 3\varphi] \cdot \sigma_{D_{3d}}^{Qr}(4, 3) \end{aligned}$$

For  $\theta = 0$ ,  $\varphi = 0$  and  $\psi = 0$ :

$$\hat{\epsilon} = \begin{pmatrix} 0 \\ 0 \\ 1 \end{pmatrix} = \hat{\epsilon}_1, \quad \hat{k} = \begin{pmatrix} 1 \\ 0 \\ 0 \end{pmatrix} = \hat{k}_1 \quad (13)$$

$$\sigma_{D_{3d}}^Q(\hat{\epsilon}_1, \hat{k}_1) = \sigma_{D_{3d}}^Q(0, 0) - \sqrt{\frac{5}{14}} \cdot \sigma_{D_{3d}}^Q(2, 0) - \frac{4}{\sqrt{14}} \cdot \sigma_{D_{3d}}^Q(4, 0) \quad (14)$$

For  $\theta = \frac{\pi}{2}$ ,  $\varphi = 0$  and  $\psi = \frac{\pi}{2}$ :

$$\hat{\epsilon} = \begin{pmatrix} 1 \\ 0 \\ 0 \end{pmatrix} = \hat{\epsilon}_2, \quad \hat{k} = \begin{pmatrix} 0 \\ 1 \\ 0 \end{pmatrix} = \hat{k}_2 \quad (15)$$

$$\sigma_{D_{3d}}^Q(\hat{\epsilon}_2, \hat{k}_2) = \sigma_{D_{3d}}^Q(0, 0) + 2 \cdot \sqrt{\frac{5}{14}} \cdot \sigma_{D_{3d}}^Q(2, 0) + \frac{1}{\sqrt{14}} \cdot \sigma_{D_{3d}}^Q(4, 0) \quad (16)$$

For  $\theta = \frac{\pi}{4}$ ,  $\varphi = 0$  and  $\psi = 0$ :

$$\hat{\epsilon} = \begin{pmatrix} \frac{1}{\sqrt{2}} \\ 0 \\ \frac{1}{\sqrt{2}} \end{pmatrix} = \hat{\epsilon}_3, \quad \hat{k} = \begin{pmatrix} \frac{1}{\sqrt{2}} \\ 0 \\ -\frac{1}{\sqrt{2}} \end{pmatrix} = \hat{k}_3 \quad (17)$$

$$\sigma_{D_{3d}}^Q(\hat{\epsilon}_3, \hat{k}_3) = \sigma_{D_{3d}}^Q(0, 0) - \sqrt{\frac{5}{14}} \cdot \sigma_{D_{3d}}^Q(2, 0) + \frac{19}{4 \cdot \sqrt{14}} \cdot \sigma_{D_{3d}}^Q(4, 0) \quad (18)$$



From equation 14, 16 and 18, we show that the E2 isotropic cross section of a trigonal crystal with a  $D_{3d}$  point group is:

$$\sigma_{D_{3d}}^Q(0, 0) = \frac{6 \cdot \sigma_{D_{3d}}^Q(\hat{\epsilon}_1, \hat{k}_1) + 5 \cdot \sigma_{D_{3d}}^Q(\hat{\epsilon}_2, \hat{k}_2) + 4 \cdot \sigma_{D_{3d}}^Q(\hat{\epsilon}_3, \hat{k}_3)}{15} \quad (19)$$

**Orthorhombic crystals.** In orthorhombic crystals with a  $D_{2h}$  point group, symmetry considerations lead to the following expression of the E2 absorption cross section (Brouder, 1990):

$$\begin{aligned} \sigma_{D_{2h}}^Q(\hat{\epsilon}, \hat{k}) = & \sigma_{D_{2h}}^Q(0, 0) \\ & + 2 \cdot \sqrt{\frac{15}{7}} \cdot \sin \theta \cdot \sin \psi \cdot [\cos \theta \cdot \sin \psi \cdot (\sigma_{D_{2h}}^{Qr}(2, 1) \cdot \cos \varphi + \sigma_{D_{2h}}^{Qi}(2, 1) \cdot \sin \varphi) \\ & + \cos \psi \cdot (\sigma_{D_{2h}}^{Qr}(2, 1) \cdot \sin \varphi - \sigma_{D_{2h}}^{Qi}(2, 1) \cdot \cos \varphi)] \\ & + \sqrt{\frac{15}{7}} \cdot [(\cos^2 \theta \cdot \sin^2 \psi - \cos^2 \psi) \cdot \sigma_{D_{2h}}^{Qr}(2, 2) \cdot \cos 2\varphi \\ & + 2 \cdot \cos \theta \cdot \sin \psi \cdot \cos \psi \cdot \sigma_{D_{2h}}^{Qr}(2, 2) \cdot \sin 2\varphi] \\ & + \sqrt{\frac{10}{7}} \cdot \sin \theta \cdot [(14 \cdot \cos^2 \theta \cdot \cos^2 \psi + 8 \cdot \sin^2 \psi - 7) \cdot \cos \theta \cdot (\sigma_{D_{2h}}^{Qr}(4, 1) \cdot \cos \varphi + \sigma_{D_{2h}}^{Qi}(4, 1) \cdot \sin \varphi) \\ & - (7 \cdot \cos^2 \theta - 1) \cdot \sin \psi \cdot \cos \psi \cdot (\sigma_{D_{2h}}^{Qr}(4, 1) \cdot \sin \varphi - \sigma_{D_{2h}}^{Qi}(4, 1) \cdot \cos \varphi)] \\ & - 2 \cdot \sqrt{\frac{5}{7}} \cdot [(7 \cdot \sin^2 \theta \cdot \cos^2 \theta \cdot \cos^2 \psi + \cos^2 \theta \cdot \sin^2 \psi - \cos^2 \psi) \cdot \sigma_{D_{2h}}^{Qr}(4, 2) \cdot \cos 2\varphi \\ & - (7 \cdot \sin^2 \theta - 2) \cdot \cos \theta \cdot \sin \psi \cdot \cos \psi \cdot \sigma_{D_{2h}}^{Qr}(4, 2) \cdot \sin 2\varphi] \\ & + \sqrt{10} \cdot \sin \theta \cdot [(1 - 2 \cdot \cos^2 \theta \cdot \cos^2 \psi) \cdot \cos \theta \cdot (\sigma_{D_{2h}}^{Qr}(4, 3) \cdot \cos 3\varphi + \sigma_{D_{2h}}^{Qi}(4, 3) \cdot \sin 3\varphi) \\ & + (3 \cdot \cos^2 \theta - 1) \cdot \sin \psi \cdot \cos \psi \cdot (\sigma_{D_{2h}}^{Qr}(4, 3) \cdot \sin 3\varphi - \sigma_{D_{2h}}^{Qi}(4, 3) \cdot \cos 3\varphi)] \\ & + \sqrt{5} \cdot \sin^2 \theta \cdot [(\cos^2 \theta \cdot \cos^2 \psi - \sin^2 \psi) \cdot \sigma_{D_{2h}}^{Qr}(4, 4) \cdot \cos 4\varphi \\ & - 2 \cdot \cos \theta \cdot \sin \psi \cdot \cos \psi \cdot \sigma_{D_{2h}}^{Qr}(4, 4) \cdot \sin 4\varphi] \end{aligned} \quad (20)$$

For  $\theta = 0$ ,  $\varphi = 0$  and  $\psi = \frac{\pi}{4}$ :

$$\hat{\epsilon} = \begin{pmatrix} 0 \\ 0 \\ 1 \end{pmatrix} = \hat{\epsilon}_1, \quad \hat{k} = \begin{pmatrix} \frac{1}{\sqrt{2}} \\ \frac{1}{\sqrt{2}} \\ 0 \end{pmatrix} = \hat{k}_1 \quad (21)$$

From equation 20, we show that the E2 isotropic cross section of an orthorhombic crystal with a  $D_{2h}$  point group is:

$$\sigma_{D_{2h}}^Q(0, 0) = \sigma_{D_{2h}}^Q(\hat{\epsilon}_1, \hat{k}_1) \quad (22)$$

### Supplemental material references

Blanchard, M., Lazzeri, M., Mauri, F. and Balan, É. (2008) First-Principles Calculation of the Infrared Spectrum of Hematite. *American Mineralogist*, 93, 1019-1027.

- Blanchard, M., Balan, É., Giura, P., Béneut, K., Yi, H., Morin, G., Pinilla, C., Lazzeri, M. and Floris, A. (2014) Infrared Spectroscopic Properties of Goethite: Anharmonic Broadening, Long-Range Electrostatic Effects and Al Substitution. *Physics and Chemistry of Minerals*, 41, 289-302.
- Blöchl, P.E. (1994) Projector Augmented-Wave Method. *Physical Review B*, 50, 17953-17979.
- Brouder, C. (1990) Angular Dependence of X-Ray Absorption Spectra. *Journal of Physics: Condensed Matter*, 2, 701-738.
- Cabaret, D., Bordage, A., Juhin, A., Arfaoui, M. and Gaudry, É. (2010). First-Principles Calculations of X-Ray Absorption Spectra at the K-Edge of 3d Transition Metals: An Electronic Structure Analysis of the Pre-Edge. *Physical Chemistry Chemical Physics*, 12, 5619-5633.
- Chassé, M., Griffin, W.L., O'Reilly, S.Y. and Calas, G. (2017) Scandium Speciation in a World-Class Lateritic Deposit. *Geochemical Perspectives Letters*, 3, 105-114.
- Chassé, M., Juhin, A., Cabaret, D., Delhommaye, S., Vantelon, D. and Calas, G. (2018) Influence of Crystallographic Environment on Scandium K-Edge X-Ray Absorption Near-Edge Structure Spectra. *Physical Chemistry Chemical Physics*, 20, 23903.
- Cornell, R.M. and Schwertmann, U. (2003) *The Iron Oxides – Structure, Properties, Reactions, Occurrences and Uses*, 2nd ed., 694 p. Wiley-VCH, Weinheim.
- Ducher, M., Blanchard, M., Vantelon, D., Nemausat, R. and Cabaret, D. (2015) Probing the Local Environment of Substitutional Al<sup>3+</sup> in Goethite Using X-Ray Absorption Spectroscopy and First-Principles Calculations. *Physics and Chemistry of Minerals*, 43, 1-11.
- Filipponi, A. (2000) Deconvolution of the Lifetime Broadening from X-Ray Absorption Spectra of Atomic and Molecular Species. *Journal of Physics B*, 33, 2835.
- Giannozzi, P., Baroni, S., Bonini, N., Calandra, M., Car, R., Cavazzoni, C., Ceresoli, D., Chiarotti, G.L., Cococcioni, M., Dabo, I., Dal Corso, A., De Gironcoli, S., Fabris, S., Fratesi, G., Gebauer, R., Gerstmann, U., Gougoussis, C., Kokalj, A., Lazzeri, M., Martin-Samos, L., Marzari, N., Mauri, F., Mazzarello, R., Paolini, S., Pasquarello, A., Paulatto, L., Sbraccia, C., Scandolo, S., Sclauzero, G., Seitsonen, A.P., Smogunov, A., Umari, P. and Wentzcovitch, R.M. (2009) QUANTUM ESPRESSO: A Modular and Open-Source Software Project for Quantum Simulations of Materials. *Journal of Physics: Condensed Matter*, 21, 395502.
- Krause, M.O. and Oliver, J.H. (1979) Natural Widths of Atomic K and L levels, K $\alpha$  X-ray lines and Several KLL Auger Lines. *Journal of Physical and Chemical Reference Data*, 8, 329-338.
- Lelong, G., Radtke, G., Cormier, L., Bricha, H., Rueff, J.-P., Ablett, J.M., Cabaret, D., Gélébart, F. and Shukla, A. (2014) Detecting Non-Bridging Oxygens: Non-Resonant Inelastic X-Ray Scattering in Crystalline Lithium Borates. *Inorganic Chemistry*, 53, 10903-10908.
- Monkhorst, H.J. and Pack, J.D. (1976) Special Points for Brillouin-Zone Integrations. *Physical Review B*, 13, 5188-5192.
- Perdew, J. P., Burke, K. and Ernzerhof, M. (1996) Generalized Gradient Approximation Made Simple. *Physical Review Letters*, 77, 3865-3868.

Rappe, A. M., Rabe, K.M., Kaxiras, E. and Joannopoulos, J.D. (1990) Optimized Pseudopotentials. *Physical Review B*, 41, 1227-1230.

Saintavit, P., Petiau, J., Benfatto, M. and Natoli, C.R. (1989) Comparison between XAFS Experiments and Multiple-Scattering Calculations in Silicon and Zincblende. *Physica B: Condensed Matter*, 158, 347-350.

### List of supplementary figures

**Figure S1** Experimental and calculated pre-edge regions of Sc K-edge XANES spectra of Sc-substituted hematite: **(a)** isolated structural model; **(b)** paired structural model. The calculated electric dipole (E1) and quadrupole (E2) contributions are displayed. The partial densities of the absorbing Sc (Sc\*) 4*p* and 3*d* states, of the first six O neighbors 2*p* states, of the first Fe and Sc neighbors 3*d* states are shown. In a matter of clarity, the DOS from the three clusters of Fe neighbors in hematite located at ca. 3.0 Å, ca. 3.4 Å and ca. 3.7 Å are averaged, due to their similarities. The energy scale of the experimental spectra is shifted to match calculated spectra. The vertical line indicates the Fermi level ( $E_F$ ). The \* symbols indicate features discussed in the paper.

**Figure S2** Comparison between experimental (red) and calculated (black) normalized Sc pre-*K*-edge XANES spectra of Sc-substituted hematite (paired structural model). Each calculated spectrum corresponds to the electric-dipole cross section for a given orientation of the polarization vector ( $\hat{\epsilon}$ ) chosen in an orthonormal reference frame bound to the crystal.